www.editada.org

International Journal of Combinatorial Optimization Problems and Informatics, 17(5), 2026, 121-137. ISSN: 2007-1558.
https://doi.org/10.61467/2007.1558.2026.v17i5.1191

Optimization of Multi-modal Relaxometry MR Acquisitions for Estimating Quantitative Brain Microstructure Parameters

Ashley Aguilar-Salinas[1], Alonso Ramírez-Manzanares[2], Ramon Ruiz-Olais[2], Carlos Segura[2].

[1] Escuela Nacional de Estudios Superiores UNAM (ENES Morelia), Mexico.

[2] Computer Science Department, Centro de Investigación en Matemáticas, A.C.

E-mails: ashaguilar06@gmail.com, alram@cimat.mx, ramon.ruiz@cimat.mx, carlos.segura@cimat.mx.

Abstract. This study addresses the optimization of MRI acquisition protocols to improve the estimation of brain microstructure descriptors, with a focus on the myelin fraction. The problem is formulated as a binary optimization task with constraints, where each decision variable encodes whether a specific repetition time is included in the protocol. Each candidate protocol is evaluated through an objective function that quantifies the relative error in the estimation of the myelin fraction. Different approximate optimization strategies were analysed, including local search and memetic algorithms with and without explicit diversity control. Under realistic acquisition conditions, population-based strategies outperformed both local search and fixed reference protocols, reducing the relative estimation error by over 30%. These findings highlight the potential of systematic optimization in MRI acquisition protocol design.

Keywords: Magnetic Resonance Imaging, Acquisition Protocol Optimization, Myelin Fraction Estimation, Memetic Algorithms, Combinatorial Optimization.

Article Info
Received October 16, 2025
Accepted Aug 16, 2026

1 Introduction

Since ancient times, human beings have sought to understand their existence and the world around them, questioning the origins of thought, emotions, behaviour, and wisdom. These concerns sparked the study of the brain, which is now recognized as one of the most complex structures in the human body. Composed of millions of neurons interconnected through axons and dendrites, this organ regulates vital functions and supports higher cognitive processes such as memory and reasoning (Manes, 2014). In antiquity, brain analysis was only possible through post-mortem dissections; over time, scientific advances made it possible to develop techniques for its study in living organisms. However, this progress faced significant technical challenges, particularly in image acquisition, due to the brain's location within the skull, a rigid bony structure, and the soft nature of neural tissue. In response to these limitations, neuroimaging techniques have revolutionized both the clinical and scientific fields, allowing the indirect recording of its structure and function through physical signals (Buxton, 2009).

Among neuroimaging techniques, magnetic resonance imaging (MRI) has become essential due to its ability to generate high-resolution anatomical and functional images without ionising radiation. Its operation is based on the interaction between magnetic fields and the protons found in biological tissues. When these protons are aligned by a magnetic field and excited by radiofrequency pulses, they emit signals detectable by the scanner's sensors, which are computationally transformed into three-dimensional representations of the human brain (Jack et al., 2015; Braskie & Thompson, 2014). Because of its non-invasive nature, versatility, and high resolution, MRI is now one of the principal tools for studying the central nervous system.

Given its wide range of clinical and research applications, MRI demands meticulous experimental planning that carefully considers the configuration of acquisition parameters, the overall protocol design, and the associated analysis strategies. These technical aspects are closely interrelated, demanding a balance between diagnostic quality, operational feasibility, and methodological consistency (Jenkinson & Chappell, 2018). In practice, key parameters such as repetition time (TR) and echo time (TE) are often set according to default values provided by the equipment. These configurations, typically derived from empirical knowledge and technological limitations, may not result from a formal optimization process.

This approach reveals an opportunity to refine acquisition protocols from a computational and systematic perspective. Although traditional settings have proven to be functional, they leave room for exploring alternatives that could improve data quality and the estimation of physiological parameters. Given the technical and multidimensional complexity involved in designing acquisition protocols in MRI, it is appropriate to address this challenge from a computational approach oriented towards efficient decision-making. In this regard, optimization emerges as a tool that offers a mathematical and computational framework to select specific configurations based on established criteria (Jiménez Lozano, 2009). Many of these problems exhibit a combinatorial nature and interaction among variables, classifying them as NP-hard, where optimal solutions are not guaranteed in a reasonable time. This limitation led to the development of heuristic methods, which, although not ensuring global optima, can provide high-quality solutions within acceptable timeframes. Among these, local search methods stand out for their applicability; they start from an initial solution and refine it iteratively until no further improvement is possible (Martí, 2004).

To overcome heuristic limitations, metaheuristics emerged as general and robust strategies capable of exploring vast search spaces, avoiding local optima, and adapting to complex problems (Osman & Kelly, 1996). Evolutionary algorithms (EAs), inspired by biological evolution, are among the most representative. These algorithms work on populations of solutions evolving through selection, recombination, and mutation, allowing parallel and flexible search (Hernández et al., 2007). Under these heuristic and metaheuristic frameworks, memetic algorithms (MAs) emerged as a promising approach that combines the global exploration of EAs with local refinement, enhancing solution quality (Moscato & Cotta, 2003). Recent developments have incorporated diversity control mechanisms into MAs to prevent premature convergence and promote a better balance between exploration and exploitation. This is especially relevant in multimodal problems like MRI protocol design. Studies such as Lugo et al. (2022) have shown that actively managing population diversity, through similarity measures, can improve the effectiveness of the optimizers.

Within this field, various studies have explored the practical application of algorithmic approaches in the context of magnetic resonance imaging. While most efforts have focused on improving the quality of the images once acquired, through reconstruction, segmentation, or artefact reduction techniques (Escorza Aguilar, 2016; Bandala Álvarez & González Pérez, 2023; Cárdenes Almeida et al., 2008), proposals have also been developed to optimize key aspects of the acquisition process, such as scan time reduction (Adria et al., 2009; Alexander, 2008), protocol parameter adjustment (Wright, Hu, & Macovsky, 1991; Wright, Nishimura, & Macovsky, 1991; Conversano et al., 2012), or the geometry of the involved devices (Tritrakarn, Takashi, & Okamura, 2024). These contributions reflect a growing interest in integrating advanced computational methodologies into the experimental design of medical imaging, aiming to improve the efficiency, precision, and clinical application of MRI studies.

Despite these advances, the studies that focused on the correct estimation of the relaxation parameters have omitted the optimization on the number of MR acquisitions, for instance, by using a fixed set of 60 MR acquisitions (Canales-Rodríguez, Pizzolato, Piredda, et al., 2021; Yu et al., 2021), and 1000 fixed for synthetic and 32 for *in vivo* data (Canales-Rodríguez, Pizzolato, Yu, et al., 2021) . This omission may limit improvements in subsequent analysis phases, where optimization is more commonly applied. Based on the above, this study hypothesises that there is still room for improvement in the selection of acquisition parameters for MRI experimental design, beyond what is achieved through configurations based on the knowledge of experts and empirical adjustments. Building on this hypothesis, this study addresses the problem at its root by adapting approximate combinatorial optimization techniques to automatically define acquisition configurations based on physiologically realistic simulations and experimental constraints. We employ both local heuristics and population-based metaheuristics, incorporating diversity control mechanisms to analyse the premature convergence issue and to improve search efficiency. The aim is to obtain robust and feasible protocols that enhance the estimation of key physiological parameters, particularly the myelin percentage, which is clinically relevant due to its association with neurodegenerative diseases. While the primary purpose of this paper is to advance the state of the art in the optimization of MRI acquisition protocols, some of the most recent methodologies in the design of memetic algorithms, including techniques to explicitly manage the diversity of the population are integrated with the aim of exploring which techniques are the most adequate for this specific problem. An important methodological advance relies on the definition of a new distance metric for binary-encoded solutions. While

this metric considers some problem-specific knowledge, it might be extended to other domains. The optimization code for our proposal is freely available at the mri-p-optimization repository (Ruiz-Olais & Aguilar-Salinas, 2026).

From this point forward, the article is structured as follows. Section 2 presents the nature of the problem and its computational formulation, addressing key aspects of MRI acquisition. Section 3 introduces a computational cost reduction strategy and describes the proposed algorithms. Section 4 reports the experimental results, comparing the performance of the proposed methods with reference protocols, with emphasis on estimation accuracy and diversity preservation in population-based algorithms. Finally, Section 5 presents the conclusions and outlines potential future research directions.

2 Problem Formulation

The development of effective methodologies for optimizing protocols used in MRI acquisition aimed at improving the estimation of parameters associated with brain microstructure constitutes the primary focus of this research. In particular, the aim is to design acquisitions that maximize the estimation quality of brain-microstructure model parameters without compromising experimental feasibility or unnecessarily extending the acquisition time.

This study focuses on the optimal data acquisition for estimating multi-compartimental tissue size compartments and the longitudinal ($T1$) and transverse ($T2$) relaxation parameters. In particular, the estimation of the percentage of myelin inside brain regions is useful for the diagnosis of multiple sclerosis (Canales-Rodríguez, Pizzolato, Piredda, et al., 2021). Each acquisition protocol is defined by a set of machine parameters, namely sets of TR and trains of TE, whose configuration directly influences the recorded signal and, consequently, the ability to estimate tissue fractions associated with myelin, intra/extracellular spaces, and cerebrospinal fluid (CSF). The optimal selection of these parameters involves a problem of combinatorial nature, subject to technical, physiological, and computational constraints.

2.1 Nature and Foundations of the MRI Acquisition Problem

MRI is a non-invasive imaging technique that allows the characterization of the physical properties of biological tissues, being particularly relevant in the study of brain structure. Its operation is based on the behaviour of hydrogen protons when subjected to a strong magnetic field. These protons align with the field and, when excited by a radiofrequency pulse, generate a signal that is captured to reconstruct the image (Buxton, 2002).

Two key machine-controlled parameters in this process are the TR, which represents the interval between two successive excitation pulses, and the TE, which is the time between the application of the pulse and the acquisition of the signal. The choice of these parameters directly influences the sensitivity of the image to certain characteristics of the biological tissue microstructure as follows. The brain tissue microstructure is composed of several compartments, which are defined in the MR context by their compartment sizes and their magnetic-interaction profiles as is detailed below. The MR signal contrasts among different tissues due to the TR and TE values are governed by their intrinsic properties, specifically their relaxation times. The $T1$ parameter describes how quickly protons realign with the magnetic field after being excited and is determined primarily by complex magnetic interactions that correlate with the intrinsic hydrogen Larmor frequency, while $T2$ reflects the rate at which protons lose precessing phase-coherence in their transverse magnetization component. These relaxation times vary depending on the magnetic interactions at a micro-scale of the tissue type (namely white matter, grey matter) and are responsible for differences in signal intensity.

The convex-combination three-compartmental model of the signal generated for the coupled $T1 - T2$ relaxation phenomenon is given by the following expressions:

$$S0_{T1}(TR) = M_0 \left[f_m \left(1 - exp(-\frac{TR}{T1_m})\right) + f_{ie} \left(1 - exp(-\frac{TR}{T1_{ie}})\right) + (1 - f_m - f_{ie}) \left(1 - exp(-\frac{TR}{T1_{csf}})\right)\right] \quad (1)$$

$$S(TE,TR) = S0_{T1}(TR)\left[f_m\, exp(-\frac{TE}{T2_m}) + f_{ie}\, exp(-\frac{TE}{T2_{ie}}) + (1-f_m-f_{ie})\, exp(-\frac{TR}{T2_{csf}})\right], \quad (2)$$

where, M_0 represents the initial magnetization of the tissue, $T1_x$ and $T2_x$ are the $T1$ and $T2$ tissue relaxation values for myelin (m), intra/extracellular (ie) and cerebrospinal fluid (csf) compartments, and f_m, f_{ie} and f_{csf} are their respective size compartments (their % of presence) within the voxel. Additionally, residual magnetization effects may be added to the signal by introducing signal oscillations due to the pulse flip-angle parameter based on the EPG formalism (Canales-Rodríguez, Pizzolato, Piredda, et al., 2021).

Synthetic signals can be generated from Equations (1) and (2). These signals can incorporate a Rician noise model, which allows the simulated signals to reproduce the characteristic bias at low SNR and the non-Gaussian error distribution observed in practice. However, there are some limitations as follows. State-of-the-art synthetic generation assumes independent, stationary noise added after the signal formation step, which means it cannot fully reproduce several scanner- and acquisition-dependent effects. For example, it generally does not capture accumulated thermal noise from the receive chain (coil/electronics) during the acquisition, which can vary across time, channels, and acquisition conditions, and can introduce structured deviations that are not well described by a simple Rician draw. Likewise, synthetic signals commonly omit geometric aberrations and other spatially varying artefacts tied to the imaging pipeline, such as B0/B1 inhomogeneities, eddy currents, motion, and reconstruction-dependent correlations, unless those mechanisms are explicitly modelled. Therefore, while synthetic signals are extremely useful for controlled experiments (e.g., stress-testing estimators, comparing protocols, or generating large labelled datasets) and can realistically reproduce Rician measurement error, they may still show small differences from real MRI data due to acquisition hardware effects and complex physical/reconstruction phenomena that are difficult to model accurately and are often acquisition-, scanner-, and site-specific.

In general, research works have focused on the optimal estimation of the relative contribution of tissue components, such as f_m, f_{ie} and f_{csf}. In particular, small f_m values (<10%) may indicate a degeneration (neuronal connectivity issues) inside the white matter. Thus, the effectiveness of a particular acquisition protocol (a set of TR and TE values) depends on its ability to enhance the contrast between these components, allowing a more accurate estimation of their fractions under real experimental conditions. Table 1 presents a summary of the parameters used in the preceding description of the model and problem formulation.

Table 1. Summary of the notation and parameters used in the multi-compartment MRI signal model.

Symbol	Description	Units / range
(M_0)	Initial tissue magnetization (baseline signal at (t=0))	Arbitrary signal units (a.u.)
($T_{1,m}$)	T1 (longitudinal) relaxation time of the **myelin** compartment	s
($T_{2,m}$)	T2 (transverse) relaxation time of the **myelin** compartment	s
($T_{1,ie}$)	T1 (longitudinal) relaxation time of the **intra-/extracellular** compartment	s
($T_{2,ie}$)	T2 (transverse) relaxation time of the **intra-/extracellular** compartment	s
($T_{1,csf}$)	T1 (longitudinal) relaxation time of the **CSF** compartment	s
($T_{2,csf}$)	T2 (transverse) relaxation time of the **CSF** compartment	s
(f_m)	Signal/volume fraction of the **myelin** compartment within the voxel	($0 \leq f_m \leq 1$) (or 0–100%)

(f_{ie})	Signal/volume fraction of the **intra-/extracellular** compartment within the voxel	($0 \leq f_{ie} \leq 1$) (or 0–100%)
(f_{csf})	Signal/volume fraction of the **CSF** compartment within the voxel	($0 \leq f_{csf} \leq 1$) (or 0–100%)

2.2 Computational Formulation of the Acquisition Problem

Given the objective of optimizing acquisition configurations to improve the estimation of brain tissue parameters, the problem was computationally formulated to represent each protocol as a candidate solution within a defined search space. First, the set of candidate repetition times, denoted as $\underline{TR}$, is established using an arithmetic sequence:

$$\underline{TR} = \{\underline{TR_i} = 100 + 200(i-1) \mid i = 1, 2, \ldots, N\}\, ms \quad (3)$$

where $N = 100$, covering a range from $100\ ms$ to $19900\ ms$. Conversely, the set of echo times remains fixed throughout the study and is formally defined as $\underline{TE}$:

$$\underline{TE} = \{\underline{TE_j} = 0.007 \cdot j \mid j = 1, 2, \ldots, 10\}\, s \quad (4)$$

This representation provides a compact and structured modeling of the solution space, facilitating the application of search and optimization techniques.

Under these definitions, each candidate protocol P is represented as a binary vector $x \in \{0,1\}^N$, where $x_i = 1$ denotes that the repetition time $\underline{TR_i}$ has been selected, while $x_i = 0$ denotes its exclusion.

Each protocol must satisfy constraints that ensure experimental feasibility and compliance with clinical conditions. The train of $\underline{TE_j}$ acquisitions occur inside the TR time frame, thus, TR is the acquisition parameter that defines the maximal time the patient spends inside the machine. For ergonomy constraints, it is always desirable to minimize this time. Then, an upper bound is imposed on the total duration of the protocol. This constraint is formally defined as:

$$\sum_{i=1}^{N} x_i \cdot \underline{TR_i} \leq T_{max} \quad (5)$$

where T_{max} represents the maximum acquisition time allowed.

2.3 Objective Function

Once the computational representation of the problem has been defined, it is necessary to establish a mechanism to quantitatively evaluate the quality of a candidate solution. For this purpose, an objective function was designed to estimate the error associated with each acquisition configuration, modelling the signal's features through a simulation for relevant physical and tissue parameters.

Given a binary vector x, the acquisition protocol P is constructed by selecting the repetition times $\underline{TR_i}$ for which $x_i = 1$. This specific subset of active repetition times is then combined with the fixed set of echo times $\underline{TE}$ to define the simulation conditions.

Based on these conditions, a synthetic signal is generated using the biophysical model (2) that incorporates relevant parameters such as the myelin fraction(f_m), intra- and extracellular water content(f_{ie}), CSF(f_{csf}), and the $T1$ and $T2$ relaxation times associated with each compartment. To evaluate the accuracy of a given P, Ground-Truth (GT) values for the myelin fraction (f_{m-GT}) are defined, which are then used to simulate the corresponding signals. Subsequently, the inverse problem is solved: given the generated signal, the value of f_m is re-estimated through the numerical optimization curve fitting using Python's curve_fit function. The estimation error is computed as the absolute difference between the estimated value (f_m) and its reference (f_{m-GT}) values, averaged over the total number of simulated voxels (v). The computational procedure is summarised in **Algorithm 1**, where, formally, the objective function for a protocol P is defined as:

$$f(P) = \frac{1}{v}\sum_{i=1}^{v} \left| f_{m,i} - f_{m-GT,i} \right|, \quad (6)$$

where P represents the acquisition protocol defined by the selected values of $\underline{TR}$ and $\underline{TE}$, $f_{m,i}$ is the estimated myelin fraction at voxel i, $f_{m-GT,i}$ is the reference value of the myelin fraction at i and v is the total number of evaluated voxels. Then, the P that minimizes (6) defines the MR-acquisition conditions that allow the best way to interrogate the brain tissue in order to accurately estimate tissue parameters, as for instance, $f_{m,i}$. Despite the fact that all tissue parameters may be relevant to diagnose diseases, we focus our methodology on the estimation of the % of myelin which has been widely used in the diagnosis of, for instance, multiple sclerosis (Canales-Rodríguez, Pizzolato, Piredda, et al., 2021).

Algorithm 1 Objective Function Evaluation.

Require: TR(set of selected repetition times), SNR(signal-to-noise ratio), seed(random seed), v(number of voxels).

// Generate v synthetic ground-truth signals S_{GT}.
for each experiment i in v **do**
  randomly generate GT tissue fractions [f_{m-GT}, f_{ie-GT}, f_{csf-GT}].
  generate relaxation times $T1$ and $T2$ for m, ie, csf.
  randomly generate a flip-angle.
  simulate signal S using f_{m-GT}, f_{ie-GT}, f_{csf-GT}, $T1$, $T2$, flip, TR, $\underline{TE}$, eqns. (1) and (2).
  add Rician noise to S using the specified SNR.
  estimate optimal f_m and the rest using curve fitting numerical optimization.
  compute the estimation error for voxel i: $|f_{m\,i} - f_{m-GT\,i}|$.
end for
Return: Mean estimation error using eq. (6).

3 Algorithmic Proposals

Memetic algorithms are one of the most successful strategies to deal with complex optimization problems (Neri & Cotta, 2012). They base their success on properly combining population-based and trajectory-based heuristics (usually a hill-climbing local search) to properly balance exploration and intensification. One of their most important drawbacks is the large number of generations required to reach high-quality solutions. Thus, they are not always feasible for solving problems with high computational cost evaluations. Taking this into account, as well as the high computational cost associated with the evaluation of MRI acquisition protocols under realistic conditions, we developed a specific strategy to reduce the simulation time without significantly affecting the analysis quality. Once this methodology is explained, the optimization methods are described. First, a local search algorithm is implemented as a standalone strategy; subsequently, to avoid local optima, this procedure is integrated into a memetic algorithm. In this memetic scheme, local search acts as a refinement operator on the offspring, so that the evolutionary process operates on locally optimized configurations. Moreover, the workflow incorporates an explicit diversity management during survivor selection to deal explicitly with the premature convergence issue.

This section details the design of these approaches, covering both the evaluation cost reduction and the optimization methods that balance global exploration with local exploitation.

3.1 Strategy to Reduce Evaluation Cost

The evaluation of each acquisition protocol *P* requires simulating its behavior across multiple tissue units, commonly referred to as voxels. These represent elementary volumes within a three-dimensional image and allow localized modeling of the MRI signal generated by different configurations. However, simulating a protocol over a large set of voxels under realistic conditions entails a high computational cost, especially when large numbers of solutions must be evaluated.

To address this difficulty, a procedure was developed to reduce the number of voxels while maintaining representative results. The strategy consisted in estimating how many voxels were sufficient to properly approximate the quality order in the relative error of myelin fraction estimation. First, 200 randomly generated acquisition protocols were evaluated with 200 voxels and sorted by quality to use them as a reference. Then, subsets of those voxels with various sizes were generated and the new rankings were compared to the reference using a distance metric. This analysis enabled the establishment of a fixed number of voxels for subsequent experiments, which allowed a significant reduction in simulation time without affecting the fidelity of the results.

3.2 Local Search Strategy

To refine individual solutions in the search space, a local search strategy based on a binary flip operator was implemented. This procedure explores the neighbourhood of a candidate configuration by evaluating small variations from its initial binary representation, accepting those changes that lead to improvements according to a specific criterion.

The *neighbourhood* of a solution is defined as the set of configurations that differ from it by exactly one variable. This choice enables a reduced yet useful neighbourhood, offering controlled exploitation without incurring high computational costs. For each solution, a random permutation of the indices is generated, and the effect of flipping each component is examined sequentially. If the new solution is feasible and provides a significant reduction in the error (more than a threshold ε), it is accepted as the new current solution. In the case of a tie, that is, if the error difference does not exceed ε, the configuration with the smallest sum of TRs is preferred. The process is repeated until no further improvements are observed in the neighbourhood. The procedure is summarised in **Algorithm 2**.

Algorithm 2 Local Search with Flip-Based Neighborhood.

Require: N(number of available repetition times), ε(threshold of improvement)
Generate a random binary solution $x \in \{0,1\}^N$
Evaluate the initial solution: $e \leftarrow f(x)$
Set improvement flag: $improvement \leftarrow True$
while $improvement = True$ **do:**
  $improvement \leftarrow False$
  $\pi \leftarrow$ random permutation of $\{1,\ldots,N\}$
  for each i en π **do**
    $x' \leftarrow$ flip the i-th variable of x
    if x' is feasible **then**
      $e' \leftarrow f(x')$
      if $e' < e - \varepsilon$ **then**
        $x, e \leftarrow x', e'$
        $improvement \leftarrow True$
        break
      else if $|e - e'| \leq \varepsilon$ *and* $\sum_{i:x'_i=1} \underline{TR}_i < \sum_{j:x_j=1} \underline{TR}_j$ **then**
        $x, e \leftarrow x', e'$
        $improvement \leftarrow True$
        break
      end if
    end if
  end for
end while
Return x, e

Despite its effectiveness in the exploitation phase, this local search strategy presents clear limitations, as will be discussed in the experimental validation section, due to its sensitivity to the initial configuration. Given the multimodal nature of the problem, the algorithm is prone to stagnation in local optima, which prevents consistently achieving high-quality solutions. This results in increased variability, where the final estimation quality is highly dependent on the starting point.

3.3 Population-Based Algorithm with and Without Diversity Control

To more effectively explore the search space and overcome the limitations of local search, a memetic algorithm was implemented. This approach combines classical population-based evolutionary mechanisms with local refinement strategies, supporting both global exploration and intensive exploitation of promising solutions (Moscato & Cotta, 2003).

The procedure begins with the generation of an initial population of random binary configurations, which are transformed into feasible protocols through a repair mechanism that randomly deselects repetition times until the total acquisition time does not exceed a predefined threshold. Each configuration is then subjected to local search using **Algorithm 2**. This step aims to improve each solution independently before initiating generational evolution, and in the case of the method that manages the population diversity explicitly, to start with a level of diversity that is not so high.

Two algorithm variants were considered to evaluate the importance of managing diversity explicitly. The first corresponds to a version without explicit diversity control, where solutions evolve using classical operators. In particular, parents are selected uniformly at random, the reproduction is based on two-point crossover (Bao & Watanabe, 2009), and the survivor selection follows generational replacement with elitism (Eiben & Smith, 2003). Note that this replacement populates the new generation with the offspring and the best individual from the previous population if it outperforms the best in the new one. This version is described in Algorithm 3. The second variant incorporates explicit diversity control through the Best Non-Penalised (BNP) strategy (Lugo et al., 2022) during survivor selection. In this second version, both the quality of the solutions and their dissimilarity with previously selected individuals are considered, to preserve underexplored regions of the search space. The version with diversity control retains the same general structure as that presented in Algorithm 3, differing only in the survivor selection step (Line 8), which is replaced by the BNP strategy (Algorithm 4). BNP is based on establishing a lower bound on the distance for acceptable solutions. Given a threshold value (D_{th}), and the current population and offspring, BNP iteratively (lines 5–22) selects the best solution that meets the condition that its distance to the nearest already-selected solutions exceeds the threshold (line 14). In Algorithm 4, DCI stands for Distance to Closest Individual and it is in charge of calculating this value (lines 6–12). Another important feature of BNP is that the threshold D_{th} is dynamic. In particular, it is reduced linearly from a starting value (D_0) at the start of the optimization process to 0 at the end (line 1). Note that $T_{Current}$ represents the elapsed optimization time and T_{total} the stopping criterion. D_0 is calculated as the mean of the pairwise distances of the initial population after applying local search. Also note that if none of the individuals meet the distance threshold, then the one with the longest distance is selected (lines 15–20).

Algorithm 3 Memetic Algorithm considering generational replacement with elitism

Require: N(size of population)
1. Generate an initial population $\hat{P}_0$ of N individuals
2. Assign $i \leftarrow 0$
3. Apply local search to each individuals in $\hat{P}_0$
4. **while** stopping criterion is not met **do**
5. Select parents from $\hat{P}_i$ using uniform random selection with replacement
6. Perform two-point crossover on the mating pool to generate offspring population O_i
7. Apply local search to each individual in O_i
8. Survivor selection strategy: generational with elitism to generate $\hat{P}_{i+1}$
9. $i = i + 1$
10. **end while**
11. **Return** the best individual found

To implement the BNP mechanism, a distance metric tailored to the problem was defined to calculate the pairwise distance between two individuals. This metric considers the actual differences between the selected TR in each solution, rather than merely their binary representations. The distance between two binary configurations x_1 and x_2 is calculated in both directions based on the active TR values.

Let $\underline{TR_1}$ and $\underline{TR_2}$ be the subsets of repetition times selected by the binary vectors x_1 and x_2 respectively. Then, the distance D is formally defined as:

$$D(x_1, x_2) = D(\underline{TR_1}, \underline{TR_2}) = \frac{1}{|\underline{TR_1}| + |\underline{TR_2}|} \left(\sum_{u \in \underline{TR_1}} \min_{v \in \underline{TR_2}} |u - v| + \sum_{v \in \underline{TR_2}} \min_{u \in \underline{TR_1}} |v - u| \right), \quad (7)$$

This metric enables a more informed comparison between configurations, capturing the degree of actual overlap among selected values. This is relevant for avoiding premature convergence during the evolutionary process.

Diversity control mechanisms such as BNP have been used in other contexts to prevent premature convergence (Lugo et al., 2022; Tang, et al., 2007). In the present study, its inclusion aims to assess whether this type of mechanism can enhance search space exploration and contribute to the stability and quality of the optimization process.

Algorithm 4 Best Non-Penalized (BNP) Survivor Selection Strategy.

Require: Population $\hat{P} = \{\hat{n}^1, \ldots, \hat{n}^N\}$, Offspring $O = \{o^1, \ldots, o^N\}$

$D_{th} = D_0 - \frac{T_{current}}{T_{total}} \times D_0$
$S_{Eligible} = \hat{P} \cup O$
$S_{Penalized} = \emptyset$
$S_{NewPopulation} = \emptyset$
while $|S_{NewPopulation}| < N$ **do**
  for $individual \in S_{Eligible}$ **do**
    $individual.dci = DCI(individual, S_{NewPopulation})$
    if $individual.dci < D_{th}$ **then**
      $S_{Eligible} = S_{Eligible} \setminus \{individual\}$
      $S_{Penalized} = S_{Penalized} \cup \{individual\}$
    end if
  end for
  if $S_{Eligible} \neq \emptyset$ **then**
    $new\_selected = argmin_{x \in S_{Eligible}} x.error$ // Ties: if $|x_1.error - x_2.error| \leq \varepsilon \rightarrow$ select individual with lowest $\sum \frac{TR}{}$
  else
    for $individual \in S_{Penalized}$ **do**
      $individual.dci = DCI(individual, S_{NewPopulation})$
    end for
    $new\_selected = argmax_{x \in S_{Penalized}} x.dci$ // Ties are broken randomly
  end if
  $S_{NewPopulation} = S_{NewPopulation} \cup \{new\_selected\}$
end while
Return $S_{NewPopulation}$

4 Results

This section presents the experimental results obtained through the application of the proposed optimization strategies. The evaluation focused on the ability of each approach to minimize the relative estimation error of the f_m parameter, under physiologically realistic conditions. To this end, representative simulation conditions were established, based on recommendations from experts in the field, allowing for a consistent comparison of the performance of the implemented methods. To ensure consistency and allow for a fair comparison among the proposed methods, uniform evaluation conditions were defined. The limit T_{max} was fixed to 50,000 ms for all experiments, the number of voxels was set to 40 in accordance with the analysis of the results presented in Section 4.1, and the local search improvement threshold ϵ was set at 0.002.

The local search logic was standardized across all implementations. Whether applied as a standalone strategy or as a refinement operator within the memetic algorithms, the local search terminates after 100 iterations or when improvements within the neighbourhood of the current solution are no longer possible. For the memetic algorithms, a population of 30 individuals and a limit of 100 generations were established. This is a relatively small population size. However, relying on smaller populations to increase the number of generations in computationally expensive problems is usually an effective strategy (León et al., 2025) to allow both exploration and exploitation. Note that due to the nature of the problem, extensive experimentation to evaluate the performance with different parameter values is not feasible. Thus, our validation is based on comparing our results against those obtained by experts.

In addition, the results of the proposed methods were compared with two fixed acquisition protocols: a reference protocol (TR_R), extracted from a clinical database provided by the Instituto de Neurobiología (INB) of the Universidad Nacional

Autónoma de México (UNAM), and an empirically derived protocol (TR_E) obtained by modifying the reference configuration to improve estimation performance. These two protocols serve as fixed baselines and are used to contextualize the performance of the proposed strategies. The corresponding repetition time values are listed below:

$$TR_R = [0.2, 0.4, 0.8, 1.5, 3.0, 5.0]s \quad \textbf{(8)}$$

$$TR_E = [0.4, 0.8, 1.5, 3.0, 5.0, 6.0, 8.0, 10.0, 12.0, 15.0, 18.0, 20.0, 25.0]s$$

Note that the empirical protocol above was not forced to comply with the constraint T_{max}.

4.1 Definition of Evaluation Conditions

Prior to evaluating the performance of the optimization strategies, simulation conditions were defined to determine a suitable number of voxels that would ensure a statistically representative analysis while reducing computational cost. This procedure is illustrated in Figure 1, which shows the distribution of ordering distances obtained from randomly generated voxel subsets, with replacement, each having a size between 1 and 50 voxels. For each size, 50 different subsets were constructed, and in each case, a new ranking of the 200 acquisition protocols was generated based on the relative error in myelin fraction estimation. The distance with respect to the reference ranking, established from the evaluation of the same 200 protocols using 200 voxels, was computed as the sum of the differences in the positions occupied by each protocol in both rankings.

As shown in Figure 1, from groups containing 40 voxels onward, the distance with respect to the reference ranking tends to stabilize and is small. This behaviour suggests that such a group size is sufficient to capture the ranking consistency of the protocols, while significantly reducing computational cost without compromising the fidelity of the analysis. A signal-to-noise ratio (SNR) of 100 was adopted, as recommended by domain experts due to its consistency with realistic experimental settings (Canales-Rodríguez, Pizzolato, Piredda, et al., 2021). Both conditions were used as a baseline for all subsequent experiments.

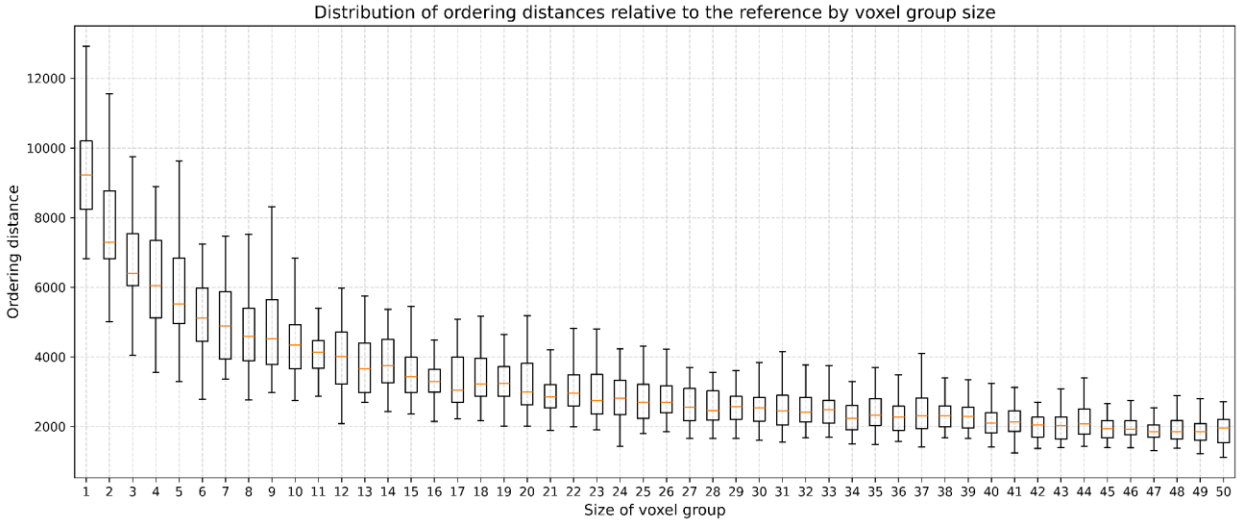

Figure 1. Distribution of distances with respect to the reference order according to the size of the voxel subset.

4.2 Analysis of the Local Search Strategy

As a first approximation, a local search strategy was applied through multiple independent runs. In each execution, an initial random solution was generated and then iteratively refined until the stopping criterion described above was met. This process was repeated 100 times, with the aim of analysing the robustness of the local search strategy for the addressed problem.

It is important to note that the relative error is bounded between 0 and 1, where values closer to zero indicate greater estimation accuracy. **Figure 2** presents the distribution of relative estimation error for the f_m parameter obtained from the independent executions. A wide dispersion of results can be observed, including outliers with errors above 0.6, which highlights the variability of the method and its susceptibility to getting trapped in local minima. Although some protocols achieved

acceptable estimations, their quality was not consistent. This behaviour led to the adoption of more robust population-based strategies, which are analysed in the following subsections.

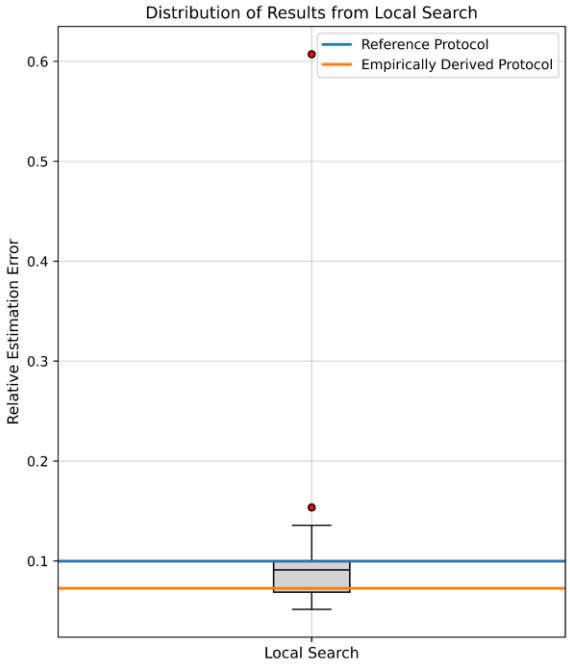

Figure 2. Distribution of the relative estimation errors for the parameter f_m obtained from the local search. The error levels achieved by the reference protocol (TR_R) and the empirically derived protocol (TR_E) are included for the reference comparison.

4.3 Memetic Algorithms with and Without Diversity Control

To overcome the limitations of local search, two variants of memetic algorithms (MAs) were implemented: one without explicit diversity control and another incorporating the BNP mechanism. Both were independently executed under the experimental conditions defined in Subsection 4.1, using an SNR of 100 and 40 voxels per evaluation. Each algorithm was run for 100 generations with a population size of 30 individuals, a constraint imposed by the high computational cost of evaluating each configuration. The stopping criterion was defined by the fixed number of generations.

The results obtained with both memetic algorithms are presented in Figure 3. The left panel displays the distribution of relative estimation errors alongside the baseline values of the two fixed protocols introduced at the beginning of Section 4: TR_R and TR_E . The right panel presents a zoomed-in comparison of both strategies, allowing a more detailed inspection. Both variants achieved similar performance, although the MA-GenElit algorithm, without explicit diversity control, tended to reach slightly lower errors. This suggests that, under the limited number of generations considered (due to the computational cost), the inclusion of the BNP mechanism did not yield improvements.

To analyse the behaviour of both memetic algorithms in greater detail, Figure 4 illustrates the evolution of the diversity, which is calculated as the mean pairwise distance. Although MA-GenElit maintained a lower level of diversity throughout the process, it exhibited no signs of premature convergence, preserving acceptable values until the end. This observation is consistent with the literature, which indicates that the advantages of explicit diversity control manifest primarily in long-term executions where standard methods tend to stagnate (Lugo et al., 2022). Given that in this study the executions were limited to 100 generations to ensure computational feasibility, the standard algorithm did not experience a critical loss of variability, explaining the comparable performance. In this context, the practical benefit of the BNP mechanism lies in enforcing a systematic management of the search, preventing abrupt drops in diversity that could compromise performance in more complex scenarios.

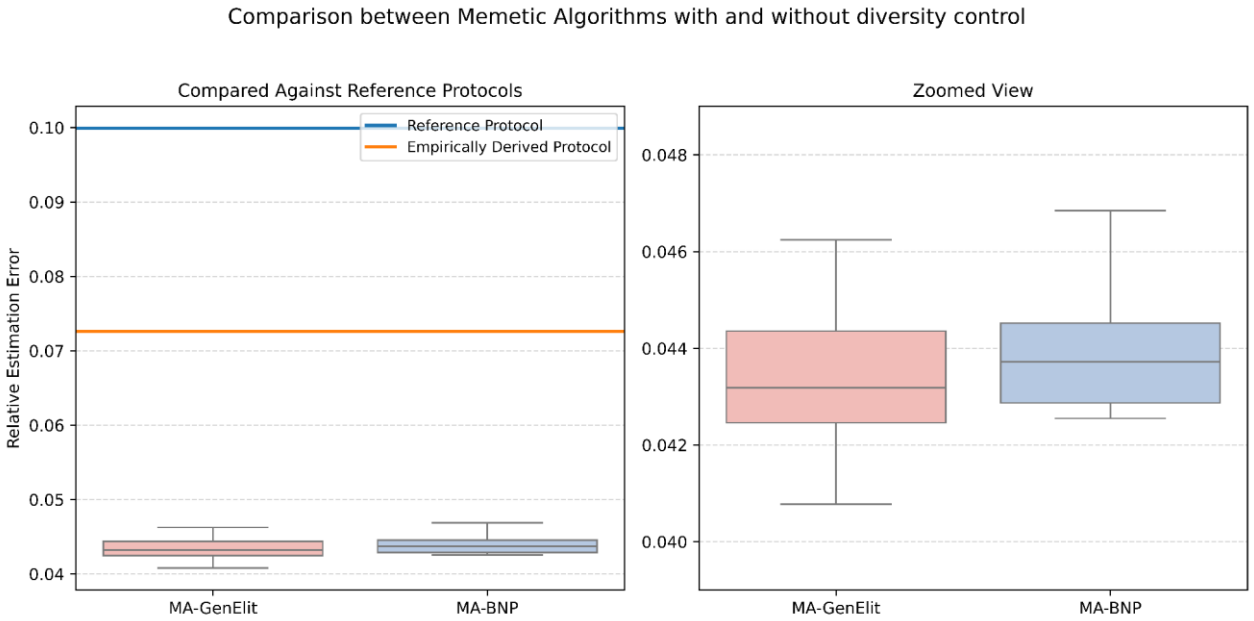

Figure 3. Comparative analysis of the relative f_m parameter estimation errors obtained by MA with and without diversity control. The left panel includes the error values corresponding to the TR_R and TR_E protocols, as horizontal baselines.
The right panel provides an enlarged view to better visualize the distributions of the proposed methods.

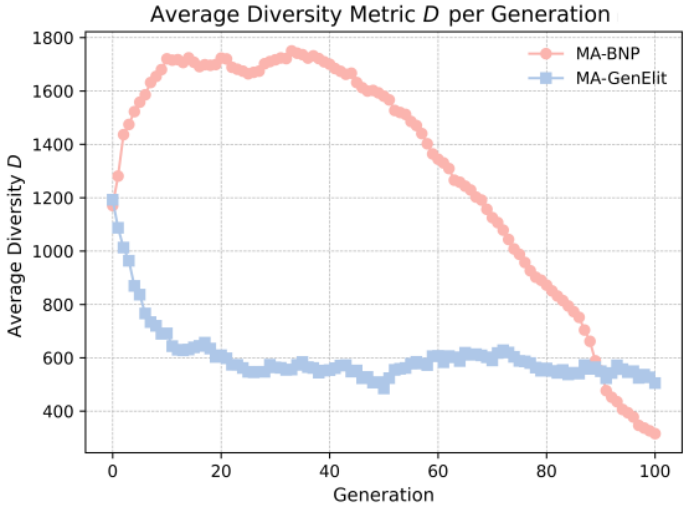

Figure 4. Evolution of the average population diversity metric D across generations for both MAs variants,
based on the distance defined in Equation (7).

4.4 Global Comparison of Optimization Strategies

Following the individual analysis of each approach, the results were integrated to perform a global comparison of the evaluated strategies. Figure 5 presents a direct comparison among the implemented methods: local search, MA-GenElit, and MA-BNP. To improve visualisation, the figure's scale was adjusted by applying a zoom that highlights the range of values with the highest representativeness within the distribution. Additionally, the figure includes the error associated with the fixed protocols TR_R and TR_E, which serve as baselines for comparison.

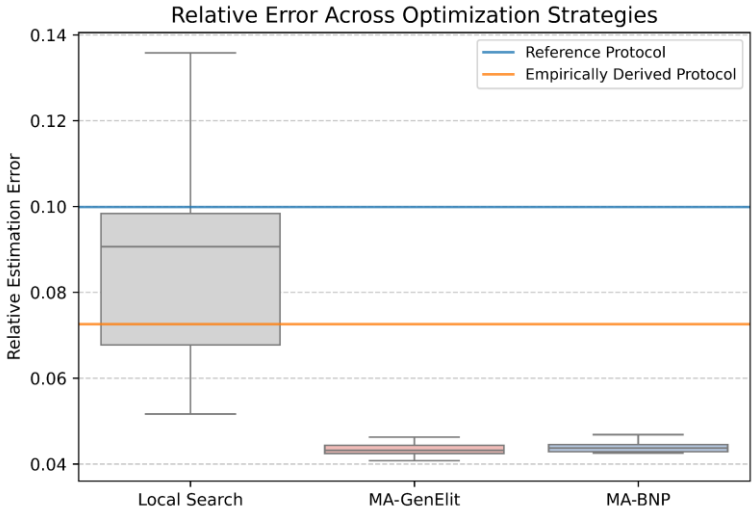

Figure 5. Global comparison of the relative f_m parameter estimation errors obtained by the applied strategies. The horizontal reference lines represent the error levels achieved by the fixed TR_R and TR_E protocols introduced above.

The results confirm that both memetic algorithms significantly outperformed the local search strategy in terms of solution quality. This improvement is attributed to the ability of population-based algorithms to explore the solution space more effectively and refine multiple configurations simultaneously. Differences between MA-GenElit and MA-BNP were minimal, suggesting that, under the tested conditions and with a limited number of generations, explicit diversity management was not essential for achieving better performance. Notably, although local search produced some acceptable estimations, it often failed to consistently outperform these fixed protocols, whereas both memetic variants clearly surpassed them. **Table 2** provides a quantitative summary of these results, detailing the minimum, maximum, mean, and standard deviation of the estimation errors for each strategy. These statistics confirm the superior robustness of the population-based approaches, as evidenced by their significantly lower standard deviations compared to local search. In particular, MA-BNP exhibited the lowest standard deviation.

The increase in precision of population-based approaches implies a higher computational cost. Although memetic algorithms demand longer execution times than standalone local search, this investment is justified by their ability to overcome local optima and consistently ensure high-quality solutions. Regarding scalability, while objective function evaluation represents the primary bottleneck, the algorithm's architecture enables the mitigation of this burden through the parallelization of population evaluations and the voxel reduction strategy. This suggests that the approach could be viable in more complex scenarios, provided that high-performance computing resources are available. In situations where more rapid optimization is required, alternative machine learning algorithms and surrogate models might be employed to improve scalability (Liu et al., 2024). However, these additional improvements fall outside the scope of this research.

Table 2. Summary of the statistical performance for the evaluated optimization strategies in terms of f_m estimation error.

Strategy	Min error	Max error	Mean error	Standard deviation
Local Search	0.0516	0.6071	0.0923	0.0552
MA-GenElit	0.0408	0.0462	0.0434	0.0015
MA-BNP	0.0426	0.0468	0.0439	0.0013

4.5 Validation of the Best Configuration Under Realistic Conditions

After completing the executions of the population-based algorithms, the configuration with the best performance for the BNP strategy was selected. The optimized acquisition protocol consists of the following repetition and echo times:

$$TR_o = [0.1, 0.3, 0.5, 0.7, 1.5, 1.7, 3.1, 3.7, 3.9, 5.7, 6.5, 7.7, 7.9]\ s \quad (9)$$

It is worth mentioning that TE values were kept fixed in all experiments $(\underline{TE})$.

The validation was carried out using an SNR of 100 and a set of 400 voxels. These conditions were established in consultation with experts in the field, as they are considered to simulate realistically the experimental scenarios commonly encountered in this type of study. The performance of the selected configuration was compared against the two fixed protocols previously introduced: TR_R, extracted from a real clinical database, and TR_E, obtained by manually improving the reference configuration through estimation feedback. The detailed performance comparison across all parameters is summarized in **Table 3.** In terms of f_m estimation, the optimized protocol clearly outperformed both baselines by reducing the relative error from 0.10 and 0.09 (for TR_R and TR_E, respectively) to 0.0675. This represents an improvement of more than 30% over the initial reference. Additionally, the number of voxels with an estimation error below 10% increased from 233 and 304 (for TR_R and TR_E, respectively) to 326 out of 400 evaluated.

Improvements were also observed in other relevant parameters, such as f_{ie}, the relaxation time $T1$, and the flip-angle. These findings indicate that the benefits of the optimized protocol extend beyond a single parameter, enhancing the characterization of brain microstructure. Moreover, this configuration maintained a robust performance when evaluated using only 40 voxels, supporting the reliability of the optimized protocol even under reduced evaluation settings.

Table 3. Estimation performance comparison among reference (TR_R), empirical (TR_E) and optimized protocols (TR_O).

	Reference protocol		Empirically derived protocol		Optimized protocol (BNP-based)	
Parameter	Relative error	# Errors<10%	Relative error	# Errors <10%	Relative error	# Errors <10%
f_m	0.10	233	0.09	304	0.0675	326
f_{ie}	0.06	336	0.02	400	0.0255	397
f_{csf}	1.26	27	0.21	32	0.6646	77
$T1_{mye}$	0.14	178	0.17	80	0.1122	225
$T2_{mye}$	0.10	242	0.01	336	0.0620	325
$T1_{ie}$	0.06	335	0.04	400	0.0298	393
$T2_{ie}$	0.07	274	0.06	368	0.0409	376
flip-angle	0.01	400	0.01	400	0.0069	400

5 Conclusions

The primary objective of this study was to reduce the relative estimation error of f_m, a key parameter for characterizing brain microstructure. Given its role in neuronal transmission and clinical relevance, particularly in neuroscience, improving its estimation represents a significant step forward in achieving more precise diagnoses based on MR imaging.

The problem was formulated as a binary optimization task with experimental constraints, allowing the evaluation of different search strategies. The initial implementation of a local search algorithm managed, in some cases, to outperform the results obtained by a reference solution TR_R (with a relative error of $f_m = 0.0998$) and an empirically derived one TR_E (with a relative error of $f_m = 0.0725$). However, the outcomes were highly variable and showed a strong tendency to become trapped in local optima, with errors reaching up to 0.6 under the experimental settings described in Section 4.1.

With the memetic algorithms, the scenario changed completely. Relative errors were observed in the range of 0.04 to 0.05, with more stable and consistent distributions. In particular, the memetic algorithm with diversity control through the BNP mechanism did not yield drastic improvements compared to the version without BNP. This aligns with what has been reported in the literature: the impact of diversity control tends to become more apparent in runs with a larger number of generations. In this study, the number of iterations was limited to ensure computational feasibility, which could explain the similarity in results. Nevertheless, using BNP did not impair the algorithm's performance, and its inclusion may be beneficial in scenarios requiring more intensive exploration. On the other hand, the memetic algorithm without BNP showed no signs of premature convergence. It maintained a good level of diversity throughout the evaluated generations, which explains why its

performance remained competitive in this particular case. This suggests that both approaches can be considered valid for this type of problem, depending on the computational resources available.

The improvement in f_m estimation with the optimized protocol indirectly benefits the estimations of other relevant parameters such as f_{ie}, $T1$, and the flip-angle because all of them are linked and related in the optimization framework. Even when the number of voxels used in the simulations was reduced, the protocol's performance remained stable, reinforcing its robustness and efficiency in resource-constrained scenarios. This work proposes a computational strategy to tune the acquisition protocol to better estimate myelin content in living brain tissue. It contributes to the field of non-invasive quantification of brain damage, providing biomarkers sensitive to neural microstructural changes associated with brain diseases. The benefit is twofold: it improves estimation accuracy and reduces the patient's scanning time.

Furthermore, the applicability of the proposed framework extends beyond the specific configuration analysed in this study. Since the set of candidate repetition times is defined via external configuration files, the method does not rely on fixed preset values. This flexibility allows the optimization strategy to be adapted to different experimental constraints or hardware limitations within the relaxometry domain, modifying the input sets of TR and TE without requiring structural changes to the algorithmic core.

These results open the door to further improvements in magnetic resonance acquisition protocols, including the incorporation of additional parameters such as echo times, or the exploration of multi-objective formulations if estimation errors across parameters are found to be uncorrelated. These strategies could also be adapted to other regions of the body, extending their clinical utility beyond the brain. Challenges remain, particularly regarding the computational cost of realistic simulations. A promising line of future work involves training predictive models, such as neural networks, to efficiently estimate the error of a given protocol without having to execute the full simulation process. This work offers a robust and technically feasible way to optimize acquisition protocols under realistic conditions. It represents a solid starting point for tackling more complex challenges at the intersection of evolutionary computation and medicine.

References

Aguilar-Salinas, A., Ramírez-Manzanares, A., Ruiz-Olais, R., & Segura, C. (n.d.). *mri-p-optimization* [Computer software]. GitHub. Retrieved September 2, 2026, from the GitHub repository.

Alexander, D. C. (2008). A general framework for experiment design in diffusion MRI and its application in measuring direct tissue-microstructure features. *Magnetic Resonance in Medicine, 60*(2), 439–448. DOI 10.1002/mrm.21646

Andria, G., Attivissimo, F., Cavone, G., & Lanzolla, A. M. L. (2009). Acquisition times in magnetic resonance imaging: Optimization in clinical use. *IEEE Transactions on Instrumentation and Measurement, 58*(9), 3140–3148. DOI 10.1109/TIM.2009.2016888

Bandala Álvarez, D., & Pérez González, J. (2023). Estimación del mapa de anisotropía fraccional y difusividad media en materia blanca utilizando transformers. *Research in Computing Science, 152*(8), 209–220.

Bao, Z., & Watanabe, T. (2009). A novel genetic algorithm with cell crossover for circuit design optimization. In *2009 IEEE International Symposium on Circuits and Systems* (pp. 2982–2985). IEEE. DOI 10.1109/ISCAS.2009.5118429

Braskie, M. N., & Thompson, P. M. (2014). A focus on structural brain imaging in the Alzheimer's Disease Neuroimaging Initiative. *Biological Psychiatry, 75*(7), 527–533. DOI 10.1016/j.biopsych.2013.11.020

Buxton, R. B. (2009). *Introduction to functional magnetic resonance imaging: Principles and techniques* (2nd ed.). Cambridge University Press. DOI 10.1017/CBO9780511605505

Canales-Rodríguez, E. J., Pizzolato, M., Piredda, G. F., Hilbert, T., Kunz, N., Pot, C., Yu, T., Salvador, R., Pomarol-Clotet, E., Kober, T., Thiran, J.-P., & Daducci, A. (2021). Comparison of non-parametric T2 relaxometry methods for myelin water quantification. *Medical Image Analysis, 69*, 101959. DOI 10.1016/j.media.2021.101959

Canales-Rodríguez, E. J., Pizzolato, M., Yu, T., Piredda, G. F., Hilbert, T., Radua, J., Kober, T., & Thiran, J.-P. (2021).

Revisiting the T2 spectrum imaging inverse problem: Bayesian regularized non-negative least squares. *NeuroImage, 244*, 118582. DOI 10.1016/j.neuroimage.2021.118582

Cárdenes Almeida, R., Muñoz Moreno, E., Tristán Vega, A., & Martín Fernández, M. (2008). Una herramienta para el procesado y visualización de imágenes de resonancia magnética de tensor de difusión. In *XXVI Congreso Anual de la Sociedad Española de Ingeniería Biomédica* (pp. 9–12).

Conversano, F., Greco, A., Casciaro, E., Ragusa, A., Lay-Ekuakille, A., & Casciaro, S. (2012). Harmonic ultrasound imaging of nanosized contrast agents for multimodal molecular diagnoses. *IEEE Transactions on Instrumentation and Measurement, 61*(7), 1848–1856. DOI 10.1109/TIM.2012.2192354

Eiben, A. E., & Smith, J. E. (2003). *Introduction to evolutionary computing*. Springer. DOI 10.1007/978-3-662-05094-1

Escorza Aguilar, A. M. (2016). *Protocolo para analizar diffusion tensor imaging (DTI) del cerebro humano* [Master's thesis, Universidad de Sevilla]. idUS.

Hernández Riveros, J. A., Dorado de la Calle, J., Gestal Pose, M., & Porto Pazos, A. B. (2007). Avances en algoritmos evolutivos. In J. J. Romero Cardalda, C. Dafonte Vázquez, Á. Gómez García, & F. J. Penousal Martins Machado (Eds.), *Inteligencia artificial y computación avanzada* (pp. 35–54). Fundación Alfredo Brañas.

Jack, C. R., Jr., Barnes, J., Bernstein, M. A., Borowski, B. J., Brewer, J., Clegg, S., Dale, A. M., Carmichael, O., Ching, C., DeCarli, C., Desikan, R. S., Fennema-Notestine, C., Fjell, A. M., Fletcher, E., Fox, N. C., Gunter, J., Gutman, B. A., Holland, D., Hua, X., . . . Weiner, M. (2015). Magnetic resonance imaging in Alzheimer's Disease Neuroimaging Initiative 2. *Alzheimer's & Dementia, 11*(7), 740–756. DOI 10.1016/j.jalz.2015.05.002

Jenkinson, M., & Chappell, M. (2018). *Introduction to neuroimaging analysis*. Oxford University Press.

Jiménez Lozano, G. (2009). *Optimización*. Universidad Nacional de Colombia, Sede Manizales.

León, G., Espinal, A., Soria-Alcaraz, J. A., & Sotelo-Figueroa, M. A. (2025). Micro differential evolution algorithm with self-adaptation for numerical optimization. In P. Melin & O. Castillo (Eds.), *Modern artificial intelligence based on soft computing techniques* (pp. 257–265). Springer. DOI 10.1007/978-3-031-88279-1_17

Liu, S., Wang, H., Peng, W., & Yao, X. (2024). Surrogate-assisted evolutionary algorithms for expensive combinatorial optimization: A survey. *Complex & Intelligent Systems, 10*(4), 5933–5949. DOI 10.1007/s40747-024-01465-5

Lugo, L., Segura, C., & Miranda, G. (2022). A diversity-aware memetic algorithm for the linear ordering problem. *Memetic Computing, 14*(4), 395–409. DOI 10.1007/s12293-022-00378-5

Manes, F. (2014). *Usar el cerebro* (4.ª ed.). Planeta.

Martí, R. (2003). Procedimientos metaheurísticos en optimización combinatoria. *Matemàtiques, 1*(1), 3–62.

Moscato, P., & Cotta, C. (2003). A gentle introduction to memetic algorithms. In F. Glover & G. Kochenberger (Eds.), *Handbook of metaheuristics* (pp. 105–144). Kluwer Academic Publishers. DOI 10.1007/0-306-48056-5_5

Neri, F., & Cotta, C. (2012). Memetic algorithms and memetic computing optimization: A literature review. *Swarm and Evolutionary Computation, 2*, 1–14. DOI 10.1016/j.swevo.2011.11.003

Osman, I. H., & Kelly, J. P. (Eds.). (1996). *Meta-heuristics: Theory and applications*. Kluwer Academic Publishers. DOI 10.1007/978-1-4613-1361-8

Tang, J., Lim, M. H., & Ong, Y. S. (2007). Diversity-adaptive parallel memetic algorithm for solving large scale combinatorial optimization problems. *Soft Computing, 11*(9), 873–888. DOI 10.1007/s00500-006-0139-6

Tritrakarn, T., Takahashi, M., & Okamura, T. (2024). Optimization of RF coil geometry for NMR/MRI applications using a genetic algorithm. *Journal of Magnetic Resonance, 362*, 107685. DOI 10.1016/j.jmr.2024.107685

Wright, G. A., Hu, B. S., & Macovski, A. (1991). Estimating oxygen saturation of blood in vivo with MR imaging at 1.5 T. *Journal of Magnetic Resonance Imaging, 1*(3), 275–283. DOI 10.1002/jmri.1880010303

Wright, G. A., Nishimura, D. G., & Macovski, A. (1991). Flow-independent magnetic resonance projection angiography. *Magnetic Resonance in Medicine, 17*(1), 126–140. DOI 10.1002/mrm.1910170117

Yu, T., Canales-Rodríguez, E. J., Pizzolato, M., Piredda, G. F., Hilbert, T., Fischi-Gomez, E., Weigel, M., Barakovic, M., Bach Cuadra, M., Granziera, C., Kober, T., & Thiran, J.-P. (2021). Model-informed machine learning for multi-component T2 relaxometry. *Medical Image Analysis, 69*, 101940. DOI 10.1016/j.media.2020.101940